# Atomic Level Modeling of Extremely Thin Silicon-on-Insulator MOSFETs Including the Silicon Dioxide: Electronic Structure

Stanislav Markov, *Member, IEEE*, Balint Aradi, Chi-Yung Yam, Hang Xie, Thomas Frauenheim, and Guanhua Chen

***Abstract*— Ultimate scaling of Si MOSFETs leads to extremely thin and short channels, which are justifiably modeled at the atomic level. Currently, hydrogen passivation of the channel is used in device models, as a compromise between efficiency and accuracy. This paper advances the state of the art by adopting a density-functional tight-binding Hamiltonian, permitting the inclusion of the confining amorphous oxide *explicitly* in the simulation domain in a way similar to *ab initio* approaches. Band structure of silicon-on-insulator films of different thicknesses is studied with this method, showing good agreement with the experiment and revealing large quantitative differences in comparison with simulations of H-passivated Si film.**

***Index Terms*— Atomistic modeling, band structure, density-functional tight binding (DFTB), oxide interface, silicon on insulator (SOI).**

## I. Introduction

ATOMIC level modeling of electronic transport in CMOS transistors is becoming increasingly relevant due to the continuous miniaturization of the technology and the recent trends in diversification of the architecture and chemical composition of devices. Numerous works evaluate the performance and scaling potential of nanowires using atomistic quantum transport, but with one notable limitation: the atomic models are hydrogen passivated, ignoring the penetration of electron wave in the gate oxide [1]–[5]. It is well known, however, that in ultrathin films and nanowires, the band structure, quantization, and interface scattering strongly depend on the amount of confinement and on the specifics of the semiconductor–oxide interface [3]–[8].

Manuscript received August 25, 2014; revised October 24, 2014; accepted December 18, 2014. Date of publication January 19, 2015; date of current version February 20, 2015. This work was supported by the University Grants Council, Hong Kong, within the Area of Excellence on Theory, Modeling and Simulation of Emerging Electronics under Contract AoE/P-04/08. The work of S. Markov was supported by the Small Project Funding Scheme through the University of Hong Kong, Hong Kong, under Project 201309176243. The review of this paper was arranged by Editor A. Schenk.

S. Markov, C.-Y. Yam, H. Xie, and G. Chen are with the Department of Chemistry, University of Hong Kong, Hong Kong (e-mail: stanislav.markov@hku.hk; yamcy@yangtze.hku.hk; xiehanggm@gmail.com; ghc@everest.hku.hk).

B. Aradi and T. Frauenheim are with the Bremen Center for Computational Materials Science, University of Bremen, Bremen 28359, Germany (e-mail: balint.aradi@bccms.uni-bremen.de; frauenheim@bccms.uni-bremen.de).

Color versions of one or more of the figures in this paper are available online at http://ieeexplore.ieee.org.

Digital Object Identifier 10.1109/TED.2014.2387288

The H-passivation of atomic models is a limitation related to simulation methodology, rather than to the lack of reliable structural models of the $Si/SiO_2$ interface. Atomistic transport is usually modeled by coupling an empirical tight binding (ETB) Hamiltonian (describing the atoms and their interactions) to the nonequilibrium Green function (NEGF) formalism (enabling the calculations of terminal currents) [1], [2]. The problem is the lack of parameterization of ETB for material interfaces with disorder and for amorphous materials, but this is what is required for modeling the $Si/SiO_2$ interface. The use of a $SiO_2$ pseudoatom to represent the oxide was proposed to circumvent the problem, but if such an approach can capture the phenomena at the interface was not explored [9]. Mapping *ab initio* density-functional-theory (DFT) Hamiltonian of the entire device to a tight binding (TB) equivalent via the maximally localized Wannier functions is also suggested, but the application beyond graphene nanoribbons remains to be seen [10]. Finally, recent advancements in overcoming the bandgap deficiency of DFT [11], [12], together with the remarkable progress in the efficiency of the DFT-NEGF schemes [13], make the *ab initio* approach attractive, but including the $SiO_2$ largely increases the number of atoms in the system, leading to extreme computational cost.

This paper reaches a milestone toward overcoming the constraint of H-passivation. Novel in our approach is the use of density-functional tight-binding (DFTB) Hamiltonian, enabling us to simulate drain current in an extremely thin silicon-on-insulator (ETSOI) transistor, including the essential part of the atoms of the gate oxide and the buried oxide (BOX) *explicitly* in the atomic model [14]. This paper is the first part of an extended report that details the methodology, demonstrates its merits, comparing the $SiO_2$- and H-passivated models, and provides additional insight toward the ultimate scaling of ETSOI devices. Here, we present the DFTB theory and band-structure calculations, consolidating the important data on confinement in ETSOI and transition of electronic structure at the $Si/SiO_2$ interface. A separate report will elaborate on the drain current simulations, confronting our model to the experiment and to the usual case of H-passivated channel.

Before we proceed with the exposition, we must clarify our choice of ETSOI architecture for the study. By ETSOI,

we envisage planar silicon-on-insulator (SOI) MOSFETs with Si-body thickness below 5 nm, be it a fully depleted or junctionless, or thin or thick BOX. Such devices are usually wide in experiments, which minimizes variability, while reliable experimental data is available for MOSFETs and for $Si/SiO_2$ superlattices down to subnanometer Si film thickness [17]–[19]. This is important for benchmarking both band structure and transport calculations. Besides, structural models of the $Si(001)/SiO_2$ interface are readily available, whereas obtaining reliable atomic models for oxidized nanowires or FinFETs presents a challenge on its own. Finally, ETSOI scaling roadmap mandates most aggressive thinning of Si, which makes the atomistic modeling including the oxide necessary, and the results could infer valuable information for FinFETs too.

## II. Methodology

### A. Density-Functional Tight-Binding (DFTB) Hamiltonian

We give an overview of DFTB theory to clarify how it fulfills the demands of efficiency and transferability for explicit treatment of the $Si/SiO_2$ interface, and what parameters are available in the theory. For the full details of DFTB, we refer the interested readers to [20]–[22].

As an approximation of DFT, DFTB is also formulated around an expression of the total energy $E$ of the atomic system as a functional of the spatial distribution of electron density $n(\boldsymbol{r})$: $E = E[n(\boldsymbol{r})]$. The electron density in DFTB is expanded in a reference density plus a small fluctuation: $n(\boldsymbol{r}) = n_0(\boldsymbol{r}) + \delta n(\boldsymbol{r})$. This is correct to second-order fluctuations in $\delta n$ [23], and enables the decomposition of the total energy in three terms

$$E = E_{\mathrm{BS}}[n_0] + E_{\mathrm{SCC}}[n_0, \delta n] + E_{\mathrm{REP}}(n_0). \tag{1}$$

The term $E_{\mathrm{BS}}$ reflects the band-structure energy arising from a Hamiltonian built on the reference density $n_0$, and is discussed in greater detail below. $E_{\mathrm{SCC}}$ captures second-order charge fluctuations due to Coulomb and some exchange–correlation (XC) interactions. It is solved with approximations in a self-consistent loop. This term is important to more accurately account for charge transfer, e.g., at semiconductor/oxide interfaces or in metal oxides with significant ionic character [24]. Finally, $E_{\mathrm{REP}}$ is the repulsive potential, arising from ion–ion interaction, double counting, and XC terms; it depends only on interatomic distances and $n_0$, and for the transport in devices with a fixed atomic structure is an irrelevant constant.

The most important term in the context of this paper is

$$E_{\mathrm{BS}} = \sum_{i}^{\mathrm{occ.}} \langle \psi_i | \hat{T} + V_{\mathrm{eff}}[n_0(\boldsymbol{r})] | \psi_i \rangle \tag{2}$$

$\hat{T}$ and $V_{\mathrm{eff}}[n_0(\boldsymbol{r})]$ being the kinetic energy operator and the Kohn–Sham effective potential. The one-electron eigenstates $\psi_i$ of the system are expanded in a linear combination of atomic orbitals (LCAO) $\{\phi_\nu\}$ centered on the atomic sites $\boldsymbol{R}_A$

$$\psi_i = \sum c_{\nu i} \phi_\nu(\boldsymbol{r} - \boldsymbol{R}_A) \tag{3}$$

$c_{\nu i}$ being the variational coefficients that minimize the energy. The LCAO expansion transforms (2) in an algebraic system for the variational coefficients

$$\sum\nolimits_\nu c_{\nu i}\left(h^0_{\mu\nu} - \varepsilon_i s_{\mu\nu}\right) = 0 \quad \forall \mu, i, \quad \text{with } \mu \in A, \nu \in B \tag{4}$$

$$h^0_{\mu\nu} = \begin{cases} \varepsilon^A_\mu, & \text{for } \mu = \nu \in A \\ & \text{and } (r_0 = \infty) \\ \langle \phi^A_\mu | \hat{T} + V^A_{\mathrm{eff}} + V^B_{\mathrm{eff}} | \phi^B_\nu \rangle, & \\ & \text{for } A \neq B \\ 0, & \text{otherwise} \end{cases} \tag{5}$$

$$s_{\mu\nu} = \langle \phi_\mu | \phi_\nu \rangle \tag{6}$$

where $h^0_{\mu\nu}$ and $s_{\mu\nu}$ are the elements of the Hamiltonian and overlap matrixes, $A$ and $B$ label different atoms in the system, and $r_0$ is defined below. The two-center approximation in (5) and nonorthogonality due to (6) are obvious.

It is important to emphasize that the atomic orbitals in (5) and (6) and the effective potentials in (5) are obtained from a self-consistent all-electron DFT calculation of the neutral atom with a confining potential of the form $(\boldsymbol{r}/r_0)^m$

$$\left[\hat{T} + V^A_{\mathrm{eff}}[n^A(\boldsymbol{r})] + (\boldsymbol{r}/r_0)^m\right]\phi_\mu = \varepsilon^A_\mu \phi_\mu(\boldsymbol{r}). \tag{7}$$

The exception is $h^0_{\mu\mu}$, obtained from free atom calculations, i.e., $r_0 = \infty$ in (7).

Two important things must be understood. First, the all-electron DFT calculation of (7) is performed only once per chemical element. Then, the matrix elements in (5) and (6) are computed and tabulated versus interatomic distance for all monoatomic and diatomic pairs, given a set of chemical elements of interest. This provides a systematic way to construct a TB Hamiltonian over a broad range of bonding configurations, including the interactions between extended neighbors, and is necessary for modeling the $Si/SiO_2$ interface.

Second to note is that the confining potential compresses the atomic orbitals and yields $V^A_{\mathrm{eff}}(\boldsymbol{r})$ and $n^A(\boldsymbol{r})$ that are better suited to represent the chemical element when bonded in a solid. The confining potential itself holds the parameters of DFTB—the confinement radius $r_0$ and the steepness of the confining potential $m$ in (7)—so that parameterization is per chemical element. This is in contrast to ETB schemes where the Hamiltonian matrix elements themselves are the fitting parameters, assuming orthogonal atomic basis, and often limiting interactions to the first nearest neighbor.

The improved transferability over ETB comes at an increased computational cost in DFTB, but the approach is still two–three orders of magnitude faster than DFT. Simulations reported here are performed with the DFTB+ code [25].

### B. Parameterization of DFTB for Modeling SOI

DFTB is parameterizable per chemical element, via the confining potential, as explained. However, publicly available parameterizations do not provide sufficient accuracy for our study [26], and we reoptimized Si parameters. We choose nine atomic orbitals to represent Si, $3s^2 3p^2 3d^0$, and use three parameters—one confinement radius per angular momentum, as detailed in Appendix A. The result of the optimization is

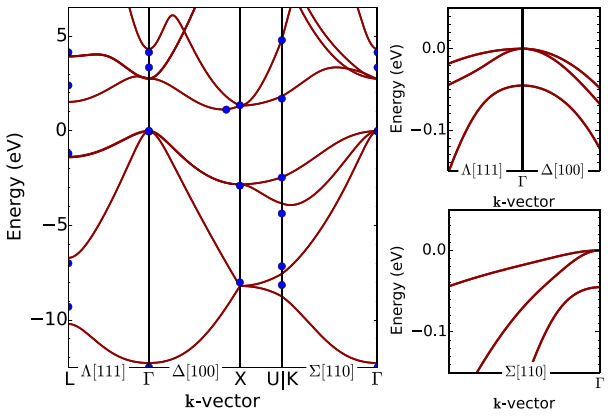


Fig. 1. Band structure of bulk Si calculated with DFTB using the parameterization obtained in this paper (lines) agree very well with the experimentally known data at the points of high symmetry (symbols) [46]. SOC is included. Si representation is $3s^2 3p^2 3d^0$ and its room temperature lattice constant of 0.543 nm is used.

TABLE I
SELECTED ENERGIES AND EFFECTIVE MASSES OF BULK SILICON

| Quantity | Target | Simulation | | Deviation |
|---|---|---|---|---|
| | | w/ SOC | w/o SOC | w/ SOC, % |
| $E_V^\Gamma$ | 0 | 0 | 0 | 0 |
| $E_C^\Gamma$ | 3.35 | 2.74 | 2.78 | –18.1 |
| $E_{C,min}^X, k_{C,min}^X$ | 1.12, 85% | 1.13, 81% | 1.14, 82% | 0.8, –4.5 |
| $E_C^L$ | 2.40 | 1.53 | 1.55 | –36.3 |
| $\Delta_{soc}$ | –0.045 | –0.045 | 0 | 0.3 |
| $m_{X,L}^E, m_{X,T}^E$ | 0.92, 0.19 | 0.95, 0.23 | 0.95, 0.23 | 3.2, 19.4 |
| $m_{[001]}^{HH}, m_{[001]}^{LH}$ | –0.28, –0.20 | –0.26, –0.15 | –0.26 | –6.2, –24.2 |
| $m_{[110]}^{HH}, m_{[110]}^{LH}$ | –0.58, –0.15 | –0.56, –0.12 | –1.1 | –3.0, –15.4 |
| $m_{[111]}^{HH}, m_{[111]}^{LH}$ | –0.74, –0.14 | –0.61, –0.12 | –0.621 | –17.3, –11.9 |
| $m^{SO}$ | –0.23 | –0.19 | - | –20.8 |

reported in Fig. 1, showing the band structure of bulk Si. The agreement with the experimentally known data from [46] at the points of high symmetry of the Brillouin zone (BZ) is very good, with an error mostly below 5%; the notable exceptions are the band minima at Γ(L) point, deviated by 18(36)%, respectively. As shown in Table I, the fundamental minimum of the conduction band along the Δ-line is well reproduced in terms of energy-momentum position, as well as in terms of band curvature, reflected in the extracted effective mass. Effective masses in the valence band are also in good agreement with the experiment. The band structure in Fig. 1 is calculated *with* spin–orbit coupling (SOC), as evidenced by the enlarged *E–k* ranges near the top of the valence band. However, as observed in Table I, simulations *without* SOC yield practically the same accuracy for the conduction band. This is advantageous, e.g., for transport simulations of n-type devices, as neglecting the SOC reduces the Hamiltonian by a factor of four.

Parameterization for O and H was not done in this paper. Instead, the confining radii reported in [27] were used in calculating the necessary matrix elements. Recently, we showed that the band structure of bulk $\alpha$-quartz $SiO_2$ is reproduced sufficiently well in this way [14], yielding a wide-bandgap insulator, as is known [28], [29]. In addition, Fig. 8 here shows the bandgap of amorphous $SiO_2$ (a-$SiO_2$)

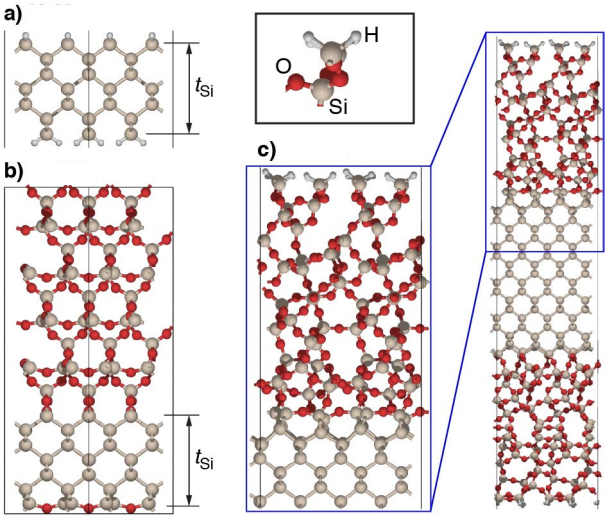


Fig. 2. Atomic models of the Si(001)/$SiO_2$ supercells used in the study, extended $2 \times 2 \times 1$ along the Cartesian directions and viewed orthographically along the [110] direction. The definition of Si film thickness is indicated for both H- and $SiO_2$-passivated Si. The different interface models are (a) H–Si, (b) $\alpha$-quartz oxide q-$SiO_2$, and (c) amorphous oxide a-$SiO_2$.

is just under 10 eV, in good agreement with the known value of 9 eV.

### C. Atomic Models

Since we are interested in the properties of ETSOI, our models must represent 2-D quantum wells consisting of thin Si film confined by $SiO_2$. Three atomic models are used in this paper, each model forming the unit cell of a tetragonal lattice, which is periodically extended along the Cartesian axes: the periodicity in $x$ and $y$ directions reflects the semi-infinite extent of the Si film parallel to the Si(001)/$SiO_2$ interface, while the periodicity in $z$—the direction of superlattice growth—permits the calculation of band structure, but is established in a way that quantum wells do not interfere.

The three unit cells are shown in Fig. 2. The simplest atomic model, labeled H–Si [Fig. 2(a)], being standard in atomic-level device modeling, is the hydrogen-passivated Si, transformed into a periodic unit cell by the addition of 10-nm vacuum buffer. Si surface is reconstructed by a $1 \times 1$ symmetric dihydrate with a 1.5-Å Si–H bond [30]. The model labeled q-$SiO_2$ [Fig. 2(b)] constitutes ∼2-nm $\alpha$-quartz $SiO_2$ attached to the crystalline Si (c-Si) via an interface layer of Si with oxygen-bridge, as in [31] and [40]. The structure has been transformed in a periodic cell by means of energy minimization within DFT, eliminating the need for vacuum buffer [7]. The most complex model, labeled a-$SiO_2$ [Fig. 2(c)], is constructed in this paper from a fragment of a-$SiO_2$/Si(001) interface, featuring the oxygen-bridge too. The interface model, obtained in [32] and [33], is connected to its mirror image after rotation by 90° around the $z$-axis, to form the $SiO_2$-Si-$SiO_2$ structure shown in Fig. 2(c); the vacuum buffer of 10 nm transforms this structure in a periodic unit cell. The interface models have been structurally relaxed in DFT; further details are given in Appendix B.

The oxide in the a-$SiO_2$ model is amorphous by virtue of lacking short-range order and having a broad dispersion in

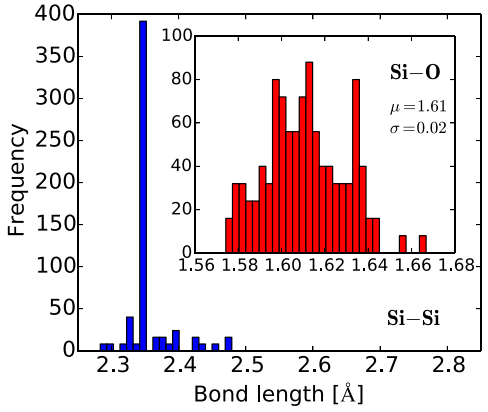


Fig. 3. Dispersion of the Si–Si and Si–O bond lengths for the a-$SiO_2$ model, reflecting the $2 \times 2 \times 1$ extended cell with ~2.5-nm Si thickness, as shown in Fig. 2(c). Dispersion of the nominal 0.235 nm for Si–Si arises from strain in the first-three layers of Si atoms. Average Si–O bond length of 1.61 Å agrees with the experimental value of 1.62 Å [49], and the range of theoretical values (1.62–1.64 Å) reported in [15].

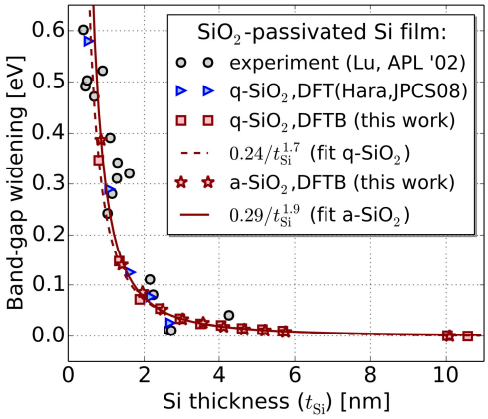


Fig. 4. Dependence of the widening of the fundamental bandgap of $SiO_2$-confined Si film on the thickness of the film. The experimental data are taken from c-Si/a-$SiO_2$ superlattice [16], while DFT calculations are reportedly from c-Si/quartz-$SiO_2$ [37]. DFTB calculations agree very well and permit reliable semiempirical fit of the dependence, as shown.

bond lengths, as observed in Fig. 3, showing the interatomic distances between first nearest neighbor Si–Si and Si–O atoms. Fig. 3 clarifies the advantage of DFTB for constructing the Hamiltonian, having the matrix elements for an arbitrary interatomic distance.

The $Si/SiO_2$ interface in our models is abrupt, through a monolayer of partially oxidized Si atoms. This is in good agreement with experimental observations of $Si^{2+}$ being the dominant suboxide species at high-quality $Si/SiO_2$ interface found in MOSFETs [47]. Although more sophisticated interface models are proposed in [34], the models deployed here are expected to yield representative electronic properties of the real $Si/SiO_2$ interface, as discussed in Appendix B. Further, they lead to a unit-cell with small lateral extent, which is advantageous in the view of our subsequent study of transport through an ETSOI channel.

The final remark concerns the construction of models that differ in Si thickness. This is accomplished by extending the c-Si core of the models with 0.8-nm Si film, as shown in Fig. 2(c). The models are partially optimized in the sense that structural relaxation is not performed after the extension of Si. This is permissible, since a previous study showed only a small change in the energy per atom, when further relaxation is done [35]. We note, however, that thinning the Si to 0.5 nm without subsequent relaxation forms electronic states in the bandgap, indicating that the confining oxides start to significantly interact through a 0.5-nm Si film.

## III. Results and Discussion

### A. Confinement Effects in Extremely Thin SOI

It is well known that 1-D confinement in Si films thinner than 5 nm leads to very significant changes in the band structure of Si [35], [36]. From the perspective of quantum mechanics, reducing the Si thickness is equivalent to the narrowing of a quantum well. Therefore, one expects enlarged separation of the energies of the molecular orbitals arising from c-Si and widening of the bandgap of the semiconductor. The dependence of the bandgap widening versus Si film thickness is shown in Fig. 4. Comparison is drawn between experimental data for a superlattice of c-Si/a-$SiO_2$ from [16] and the simulations of our models with alpha-quartz (q-$SiO_2$) and a-$SiO_2$) oxides. The simulations of a quartz-based model in DFT, as reported in [37], are also shown. The agreement between the two levels of theory and experimental data, as well as between the two model structures of the oxide, is notably good. We have also obtained semiempirical fits to our results, as shown with lines in Fig. 4. Recall that an expression $A/t_{Si}^2$ ($A$ being a fitting parameter) for the bandgap widening has been established based on an analytical argument in [36]. Here, we show that the dependence is weaker than inverse square of Si thickness. The overestimation in the analytical model owes to the assumptions of rigid $SiO_2$ potential barrier, which is not true, as we show later in this paper. We note that at mere seven layers of Si (0.8–0.9 nm), the bandgap is still below 1.5 eV.

With respect to the barrier, it appears that the simpler atomic model (q-$SiO_2$) with the semicrystalline oxide already captures the confining properties of the oxide. This fact is likely due to the structure of the $Si/SiO_2$ interface via a monolayer of $Si^{2+}$ suboxide featuring an oxygen bridge, common to both atomic models. Indeed, it was suggested that beyond the suboxide, $SiO_2$ acts as a virtually impenetrable barrier [35]. However, an alternative DFT study deploying single $SiO_4$ tetrahedra as terminating units of Si films failed to reproduce the above experimental data [38]. The calculated bandgap widening was largely overestimated, and was in better agreement with the experiments of amorphous-$Si/SiO_2$ superlattice, where the interface is supposedly rich in hydrogen-terminated dangling bonds.

This brings our discussion to Fig. 5, showing the bandgap widening versus Si film thickness in the case of hydrogen termination, i.e., the H–Si model. Such a model is an idealization, and therefore, we show only theoretical results. Again, we have a very good agreement between DFTB and the *ab initio* DFT results, as reported in [37] and [39], and the dependence is qualitatively the same as in the case

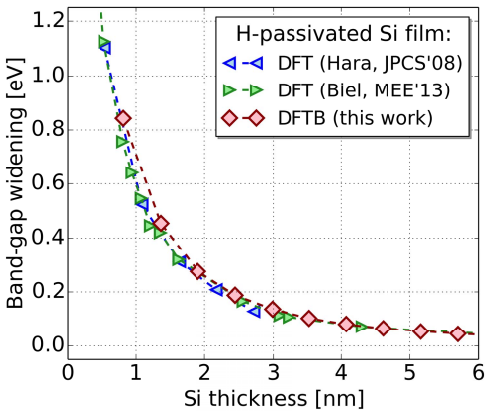


Fig. 5. Dependence of the widening of the fundamental bandgap of H-confined Si film on the thickness of the film; the DFT results are taken from [37] and [39]. Hydrogen passivation leads to much stronger confinement and the bandgap widening is more than two times larger than in the case of $SiO_2$ confinement.

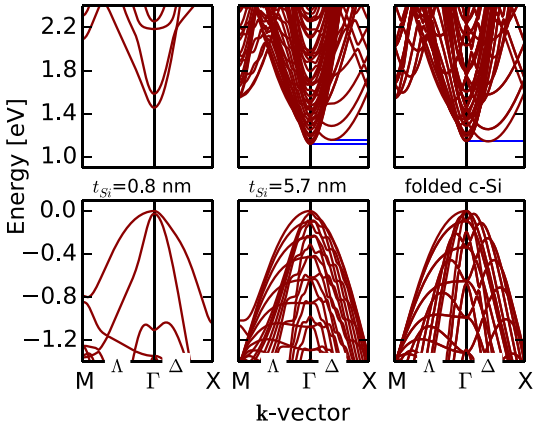


Fig. 6. Change in the band structure of extremely thin Si film ($t_{Si}$ = 0.8 and 5.7 nm) confined by $SiO_2$ q-$SiO_2$), compared with the band structure of bulk Si (folded c-Si). Note that bulk Si here is represented by a tetragonal supercell model of c-Si with the dimensions of the Si (5.7 nm)/$SiO_2$ supercell. Therefore, it exhibits the effects of BZ folding.

of $SiO_2$ confinement. However, noting the scale of the axis in Fig. 5, it becomes clear that hydrogen termination of Si overestimates the bandgap widening of the semiconductor more than twice.

Beyond bandgap widening, strong confinement of Si changes the character of its band structure too, transforming it to a direct bandgap semiconductor. This is true not only for Si nanowires and quantum dots but also for extremely thin Si films too, and is recognized as the principle reason behind enhanced photoluminescence from $Si/SiO_2$ superlattices [16], [35], [36]. In Fig. 6, we show the bottom of the conduction band and the top of the valence band of the q-$SiO_2$ supercells with 0.8- and 5.7-nm Si thickness. The striking difference between the two results from two things—confinement and BZ folding. To discriminate the effects of BZ folding, we construct a supercell of the same dimensions as the supercell with 5.7-nm Si, but fill its entire volume with c-Si. The calculated band structure of this model is also shown in Fig. 6, and referred to as folded c-Si. The band structure at 5.7 nm closely resembles that of folded c-Si, with a slight

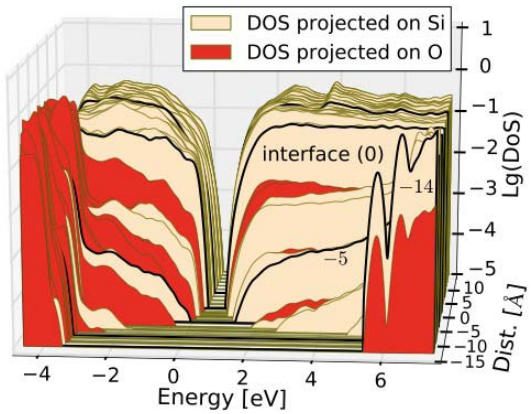


Fig. 7. On-atom projected DOS across the $Si/SiO_2$ interface, showing the gradual widening of the bandgap within the oxide. Dark/light polygons represent the DOS versus energy projected on O/Si atoms as indicated. Highest Occupied Molecular Orbital is used as energy reference. Polygons are displaced according to the distance of the corresponding atom from the interface; the atoms at negative distance are in the oxide. Thicker polygon borders identify atoms at 0.5, 0, −0.5, −1.0, and −1.4 nm from the interface.

upshift of 33 meV in the minimum of the conduction band along the Δ-line. At 0.8-nm Si, the Δ-minimum is completely missing, however. In our calculations, it is not present at 1.4-nm Si either, and is very shallow at 1.9-nm Si, where it is elevated ∼300-meV above the minimum at the center of the BZ at Γ. These findings are in excellent qualitative and quantitative agreement with earlier DFT calculations, and confirm that Δ-minimum appears only after ∼1.5-nm Si film thickness [35], [40], in contrast to an H-Si model, which was found to exhibit a Δ-minimum no matter how thin the Si [40]. We confirm also that at 10-nm Si film thickness, the band structure of the superlattice appears alike to the one of the folded c-Si.

### *B. Transition at the Si/$SiO_2$ Interface*

In the last paragraphs of this section, we discuss the nonabrupt transition of electronic structure across the $Si/SiO_2$ interface, which has occupied considerable interest in the past. The impact of the transition in MOS devices has been analyzed in [6], [7], and [41]. Here, we reveal the impact of the transition on bandgap variation in the case of SOI films.

An evocative picture of the transition of electronic structure is shown in Fig. 7. The logarithm of the density of states (DOS) versus energy, projected on each atom around the interface, is shown as a filled polygon and displaced by the distance of the atom from the $Si/SiO_2$ interface. Atoms with negative distance are in $SiO_2$; the simulated model is a-$SiO_2$ at Si thickness of ∼6 nm, which is thick enough to exhibit bulk-like character; and the highest occupied molecular orbital is used as energy reference. It is notable that the full extent of insulator bandgap, free of electronic states, opens only after about a nanometer from the interface. This is in contrast to the conventional picture of the abrupt change in the bandgap at the interface. In fact, it takes about 0.5 nm for the DOS to decay a 1000 times from the value in the c-Si film.

From the data presented in Fig. 7, we evaluate the variation of the conduction band edge (CBE)

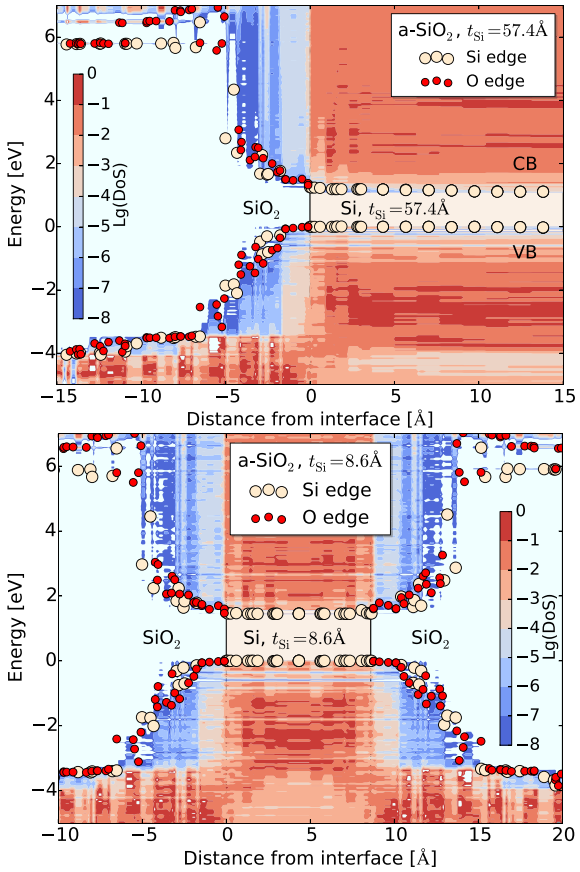


Fig. 8. Variation of the conduction and VBE around the $Si/SiO_2$ interface, extracted from the on-atom projected DOS (APDOS) for the model with amorphous silica (a-$SiO_2$), for two thicknesses of the Si film, as indicated. Bandgap is 1.12/1.45 eV for the thick/thin Si film. The colormap is a logarithm of the APDOS, showing that despite the slow initial opening of the band edges to form an insulating gap, the actual density of states is at least 10 times lower in the interfacial region than in the Si film. Light background colors delimit the Si region from the oxide.

and valence band edge (VBE) across the interface. We define the local band edge from the requirement that the number of states between the midgap of the semiconductor and the band edge is no larger than a threshold of $2 \times 10^{-4}$ on every atomic site. The approach was used also in [31] and [42], with different thresholds. While the threshold value was not justified in earlier studies, it is well defined here. Specifically, with the selected threshold, the bandgap of the c-Si obtained as $E_{\mathrm{CBE}} - E_{\mathrm{VBE}}$ equals the bandgap obtained from the band-structure calculations, $E_{\mathrm{LUMO}} - E_{\mathrm{HOMO}}$, at a given Si thickness.

The results of the extracted bandgap profile versus distance from the interface are shown in Fig. 8(a) and (b) for the cell with thick Si of 5.7 nm and in for the ETSOI of 0.9 nm, respectively. Analyzing first the case of thicker Si, we note that the bandgap in the first 0.3 nm of the oxide differs only slightly from that of Si, followed by a rather sharp transition at around 0.5 nm within the oxide. This feature has been suggested by advanced spectroscopic studies of the $Si/SiO_2$ interface in [43], and later explained to be due to the stronger dependence of the gap on the number of oxygen second nearest neighbors of a given oxygen atom, rather than on the presence of any particular type of suboxide species [44]. This aspect is well reflected in Fig. 8, which resolves the different atomic species, noting that the first oxygen atoms to the left of the interface are the oxygen bridges, with mostly Si being their second- as well as first-nearest neighbor. Fig. 8 shows unprecedented resolution in profiling the band-edge variation, owing to the a-$SiO_2$ structure having broader dispersion of bond lengths than models with semicrystalline $SiO_2$. However, the results from the q-$SiO_2$ model are very similar [14]. It is worth noting that if we vary the above mentioned DOS-threshold value to $10^{-3}$ or $10^{-6}$, we get correspondingly a more linear-like overall transition (as in [31]) or a narrower Si-like gap to about 0.7–0.8 nm, followed by an abrupt transition, (as in [7], [41], and [42]) respectively. In such cases, however, we do not recover the Si bandgap corresponding to a given Si thickness, so in our opinion, the CBE/VBE variation reported in Fig. 8 is the most realistic profile suited for phenomenological models.

Fig. 8(b) shows the band-edge profiles in the case of extremely thin Si of 0.9 nm. Due to the Si bandgap being enlarged by nearly 0.4 eV, the initial transition appears even slower, more obviously so for the CBE. Therefore, in ETSOI devices, the effect of gradual formation of the insulator gap may have stronger influence on inversion carrier density and distribution. Note that in the first half-nanometer, the bandgap barely changes by a few hundred millielectron volts, which is of the order of the lowest quantization levels (200–300 meV) in the inversion layer of a well-scaled MOSFET.

One way to account for the slow initial change of the bandgap in phenomenological models is to assume a larger Si thickness. Comparing Figs. 4 and 5, we observe that for a given Si thickness, an H–Si model with approximately 1.5 nm thicker Si yields reasonably close bandgap widening. However, the electron density in the region of the oxide, where gap transition happens, cannot be evaluated using the same 2-D DOS as in the c-Si. Figs. 7 and 8 suggest that at least an order of magnitude lower 2-D DOS must be used instead.

## IV. Conclusion

Explicit modeling of the $Si/SiO_2$ interface, including nearly 1 nm of the oxide in atomistic simulations of ETSOI devices, is necessary if quantitative accuracy is pursued. DFTB theory offers a straightforward way to build an effective Hamiltonian, and is now parameterized to yield high-accuracy band structure for the $Si/SiO_2$ system. Three important phenomena in ETSOI—bandgap widening of Si, transition to direct bandgap, and nonabrupt variation of the bandgap across the $Si/SiO_2$ interface—were reproduced by the model with a very good quantitative agreement to the experiment and *ab initio* theory. In contrast, H-passivated models of Si overestimates the confinement effects by a factor of two, yielding ~2-eV bandgap of 0.8-nm SOI, while the actual value is ~1.5 eV.

The efficiency of DFTB allowed us to explore atomic models with sufficiently thick Si to reproduce bulk-like properties, in addition to the ETSOI phenomena. We consolidated and expanded the data known from previous studies regarding extremely thin Si films, and provided reliable empirical fits for the bandgap widening versus Si film

thickness and for the bandgap transition at the interface. We hope such data will serve as a basis to enhance relevant compact models, drift–diffusion simulations, or even to parameterize a $SiO_2$ pseudoatom within the context of ETB, for SOI devices with Si below 5 nm.

## Appendix A
## DFTB Parameterization for Si

The atomic basis of Si being of $s$, $p$, and $d$ orbitals, we used one confinement radius per angular momentum as parameters, keeping the steepness of the confining potential at 4. Optimization was done with an in-house-built particle-swarm optimizer written in the Python language, including the DEAP library of evolutionary algorithms [45]. The approach is appropriate since a relationship between band structure and confinement radii of the atomic orbitals cannot be known analytically. Band structure was obtained from the primitive cell of Si, using $14 \times 14 \times 14$ $\boldsymbol{k}$-space sampling to obtain the average electron density. SOC was neglected during the optimization, accelerating the process. A subset of experimental $E-\boldsymbol{k}$ points and effective masses served as optimization targets. Optimized confinement radii for $s$, $p$, and $d$ orbitals are 3.45, 6.44, and 7.67 Bohr.

## Appendix B
## Details of the $Si/SiO_2$ Interface Models

We used published atomic models of the $Si/SiO_2$ interface in this paper [7], [33], but for completeness, we state a few details related to their construction and optimization in DFT, as well as for the relevance of their structural properties.

For the q-$SiO_2$ interface, the starting point is a hexagonal unit cell of $\alpha$-quartz $SiO_2$, which has an edge $c$ (5.41 Å) perpendicular to the other two edges of the same length $a$ (4.91 Å). This unit cell is oriented so that one of the $a$ edges and the $c$ edge are aligned with the [100] and [010] directions, respectively, and both $a$ and $c$ are matched to the Si lattice constant of 5.43 Å, permitting its attachment to c-Si. The resulting strain in the oxide is relaxed in DFT by standard techniques, with computational details given in [7] and [40]. Only the atoms of the oxide and the interfacial $Si^{+2}$ atoms are permitted to move, the c-Si atoms being fixed.

For the a-$SiO_2$ interface model, the structure is constructed by attaching strained cristobalite $SiO_2$ to c-Si. The resulting atomic system is represented as a continuous random network of bonds that connect the atoms. Subsequently, the possible defect-free equilibrium bonding configurations (network topologies) are explored via the Monte Carlo sampling. Energy-cost minimization is performed for each topology according to an expression for the total energy that includes the cost of bond length and bond-angle distortion and suboxide formation, as detailed in [32]. The optimal interface bonding is further relaxed in DFT [33], including the first three atomic layers in Si, which have off-equilibrium position, as observed from the Si–Si bond-length histogram in Fig. 3.

The resulting a-$SiO_2$ model features only $Si^{+2}$ suboxide species, as in the case of q-$SiO_2$. These were shown in [32] to be the key moiety for minimizing strain at the interface. The absence of $Si^{+3}$ and $Si^{+1}$ species is a reasonable idealization since experimental observations suggest a relatively small amount ($\sim$30%) of $Si^{+1}$ are present at the interface—composed of mainly $Si^{+2}$—while the almost fully oxidized $Si^{+3}$ species are found only beyond the interfacial layer in similar quantity [47]. Further, it has been theoretically established that $Si^{+1}$ and $Si^{+3}$ arise from entropy effects within microscopic ordered surface domains and at the boundaries of such domains without altering the ordered O-bridge-bonded topology of the interface [32], [48]. Therefore, it is justifiable to expect that the electronic and dielectric properties emerging from the structural models adopted in our study are representative for the real $Si/SiO_2$ interface. Indeed, a quantitatively very similar picture for the transition of electronic properties at the interface emerges from models including the suboxides in correct proportion, as reported in [50].

## Acknowledgment

The authors would like to thank P. Sushko of University College of London, and L. Liu of Nano Academic Technologies and Y. Wang of the University of Hong Kong for the atomic structures of the q-$SiO_2$, and a-$SiO_2$ models, respectively.

## References

[1] M. Luisier, A. Schenk, W. Fichtner, and G. Klimeck, "Atomistic simulation of nanowires in the $sp^3d^5s^*$ tight-binding formalism: From boundary conditions to strain calculations," *Phys. Rev. B*, vol. 74, no. 20, p. 205323, 2006.

[2] S. R. Mehrotra, S. Kim, T. Kubis, M. Povolotskyi, M. S. Lundstrom, and G. Klimeck, "Engineering nanowire n-MOSFETs at $L_g < 8$ nm," *IEEE Trans. Electron Devices*, vol. 60, no. 7, pp. 2171–2177, Jul. 2013.

[3] C. Y. Yam *et al.*, "A multi-scale modeling of junctionless field-effect transistors," *Appl. Phys. Lett.*, vol. 103, no. 6, p. 062109, 2013.

[4] N. Mori *et al.*, "Nano-device simulation from an atomistic view," in *Proc. IEEE IEDM*, Dec. 2013, pp. 5.1.1–5.1.4.

[5] K. Stokbro, A. Blom, and S. Smidstrup, "Atomistic simulation of a III–V p-i-n junction: Comparison of density functional and tight-binding approaches," in *Proc. Int. Conf. Simulation Semiconductor Process. Devices (SISPAD)*, Glasgow, U.K., 2013, pp. 380–383.

[6] H. Watanabe, D. Matsushita, and K. Muraoka, "Determination of tunnel mass and physical thickness of gate oxide including poly-$Si/SiO_2$ and $Si/SiO_2$ interfacial transition layers," *IEEE Trans. Electron Devices*, vol. 53, no. 6, pp. 1323–1330, Jun. 2006.

[7] S. Markov *et al.*, "Si-$SiO_2$ interface band-gap transition—Effects on MOS inversion layer," *Phys. Status Solidi A*, vol. 205, no. 6, pp. 1290–1295, 2008.

[8] D. Lizzit, D. Esseni, P. Palestri, and L. Selmi, "Surface roughness limited mobility modeling in ultra-thin SOI and quantum well III–V MOSFETs," in *Proc. IEEE IEDM*, Dec. 2013, pp. 5.2.1–5.2.4.

[9] S. Kim, M. Luisier, A. Paul, T. B. Boykin, and G. Klimeck, "Full three-dimensional quantum transport simulation of atomistic interface roughness in silicon nanowire FETs," *IEEE Trans. Electron Devices*, vol. 58, no. 5, pp. 1371–1380, May 2011.

[10] S. Bruzzone, G. Iannaccone, N. Marzari, and G. Fiori, "An open-source multiscale framework for the simulation of nanoscale devices," *IEEE Trans. Electron Devices*, vol. 61, no. 1, pp. 48–53, Jan. 2011.

[11] M. Ribeiro, L. R. C. Fonseca, and L. G. Ferreira, "Accurate prediction of the $Si/SiO_2$ interface band offset using the self-consistent *ab initio* DFT/LDA-1/2 method," *Phys. Rev. B*, vol. 79, no. 24, p. 241312, 2009.

[12] F. Tran and P. Blaha, "Accurate band gaps of semiconductors and insulators with a semilocal exchange-correlation potential," *Phys. Rev. Lett.*, vol. 102, no. 22, p. 226401, 2009.

[13] J. Maassen, M. Harb, V. Michaud-Rioux, Y. Zhu, and H. Guo, "Quantum transport modeling from first principles," *Proc. IEEE*, vol. 101, no. 2, pp. 518–530, Feb. 2013.

[14] S. Markov, C. Yam, B. Aradi, G. Penazzi, T. Frauenheim, and G. Chen, "Towards atomic level simulation of electron devices including the semiconductor-oxide interface," in *Proc. Int. Conf. Simulation Semiconductor Process. Devices (SISPAD)*, Yokohama, Japan, Sep. 2014, pp. 65–68.
[15] A. Korkin, J. C. Greer, G. Bersuker, V. V. Karasiev, and R. J. Barlett, "Computational design of $Si/SiO_2$ interfaces: Stress and strain on the atomic scale," *Phys. Rev. B*, vol. 73, no. 16, p. 165312, 2006.
[16] Z. H. Lu and D. Grozea, "Crystalline $Si/SiO_2$ quantum wells," *Appl. Phys. Lett.*, vol. 80, no. 2, pp. 255–257, 2002.
[17] A. Khakifirooz *et al.*, "Scalability of extremely thin SOI (ETSOI) MOSFETs to sub-20-nm gate length," *IEEE Electron Device Lett.*, vol. 33, no. 2, pp. 149–151, Feb. 2012.
[18] S. Migita, Y. Morita, M. Masahara, and H. Ota, "Electrical performances of junctionless-FETs at the scaling limit (LCH = 3 nm)," in *Proc. IEEE IEDM*, Dec. 2012, pp. 8.6.1–8.6.4.
[19] T. Mizuno, K. Tobe, Y. Maruyama, and T. Sameshima, "Experimental study of silicon monolayers for future extremely thin silicon-on-insulator devices: Phonon/band structures modulation due to quantum confinement effects," *Jpn. J. Appl. Phys.*, vol. 51, no. 2S, p. 02BC03, 2012.
[20] M. Elstner *et al.*, "Self-consistent-charge density-functional tight-binding method for simulations of complex materials properties," *Phys. Rev. B*, vol. 58, no. 11, pp. 7260–7268, Nov. 1998.
[21] T. Frauenheim *et al.*, "Atomistic simulations of complex materials: Ground-state and excited-state properties," *J. Phys., Condensed Matter*, vol. 14, no. 11, pp. 3015–3047, 2002.
[22] P. Koskinen and V. Mäkinen, "Density-functional tight-binding for beginners," *Comput. Mater. Sci.*, vol. 47, no. 1, pp. 237–253, 2009.
[23] W. Foulkes and R. Haydock, "Tight-binding models and density-functional theory," *Phys. Rev. B*, vol. 39, no. 17, p. 12520, 1989.
[24] G. Dolgonos, B. Aradi, N. H. Moreira, and T. Frauenheim, "An improved self-consistent-charge density-functional tight-binding (SCC-DFTB) set of parameters for simulation of bulk and molecular systems involving titanium," *J. Chem. Theory Comput.*, vol. 6, no. 1, pp. 266–278, 2010.
[25] B. Aradi, B. Hourahine, and T. Frauenheim, "DFTB+, a sparse matrix-based implementation of the DFTB method," *J. Phys. Chem. A*, vol. 111, no. 26, pp. 5678–5684, 2007. [Online]. Available: http://www.dftb-plus.info
[26] (Jan 2015). *The DFTB Website*. [Online]. Available: http://www.dftb.org
[27] M. Wahiduzzaman *et al.*, "DFTB parameters for the periodic table: Part 1, electronic structure," *J. Chem. Theory Comput.*, vol. 9, no. 9, pp. 4006–4017, 2013.
[28] L. A. J. Garvie, P. Rez, J. R. Alvarez, P. R. Buseck, A. J. Craven, and R. Brydson, "Bonding in alpha-quartz ($SiO_2$): A view of the unoccupied states," *Amer. Mineral.*, vol. 85, nos. 5–6, pp. 732–738, 2000.
[29] E. K. Chang, M. Rohlfing, and S. G. Louie, "Excitons and optical properties of alpha-quartz," *Phys. Rev. Lett.*, vol. 85, no. 12, pp. 2613–2616, 2000.
[30] J. E. Northrup, "Structure of Si(100)H: Dependence on the H chemical potential," *Phys. Rev. B*, vol. 44, no. 3, pp. 1419–1422, 1991.
[31] T. Yamasaki, C. Kaneta, T. Uchiyama, T. Uda, and K. Terakura, "Geometric and electronic structures of $SiO_2$/Si (001) interfaces," *Phys. Rev. B*, vol. 63, no. 11, p. 115314, 2001.
[32] Y. Tu and J. Tersoff, "Structure and energetics of the $Si\text{-}SiO_2$ interface," *Phys. Rev. Lett.*, vol. 84, no. 19, pp. 4393–4396, 2002.
[33] L. Lei, D. Waldron, V. Timochensky, and H. Guo, "Automistic modeling of direct tunnelling in metal-oxide-semiconductor nanostructures," in *Proc. 8th ICSICT*, Oct. 2006, pp. 1415–1418.
[34] A. Pasquarello, M. S. Hyberstsen, and R. Car, "Structurally relaxed models of the Si(001)–$SiO_2$ interface," *Appl. Phys. Lett.*, vol. 68, no. 5, pp. 625–627, 1996.
[35] P. Carrier, L. J. Lewis, and M. W. C. Dharma-wardana, "Optical properties of structurally relaxed $SiO/SiO_2$ superlattices: The role of bonding at interfaces," *Phys. Rev. B*, vol. 65, no. 16, p. 165339, 2002.
[36] E. G. Barbagiovanni, D. J. Lockwood, P. J. Simpson, and L. V. Goncharova, "Quantum confinement in Si and Ge nanostructures," *J. Appl. Phys.*, vol. 111, no. 3, p. 034307, 2012.
[37] T. Hara, Y. Yamada, T. Maegawa, and H. Tsuchiya, "Atomistic study on electronic properties of nanoscale SOI channels," *J. Phys., Conf. Ser.*, vol. 109, no. 1, p. 012012, 2008.
[38] M. Nishida, "Theoretical study of quantum-confined band-edge shifts and radiative lifetimes in oxidized Si(001) quantum films: Comparison with experiment for $Si/SiO_2$ quantum wells," *Solid State Commun.*, vol. 125, no. 10, pp. 537–542, 2003.
[39] B. Biel, L. Donetti, A. Godoy, and F. Gámiz, "*Ab initio* validation of continuum models parametrizations for ultrascaled SOI interfaces," *Microelectron. Eng.*, vol. 109, pp. 286–289, Sep. 2013.
[40] P. V. Sushko and A. L. Shluger, "Electronic structure of insulator-confined ultra-thin Si channels," *Microelectron. Eng.*, vol. 84, nos. 9–10, pp. 2043–2046, 2007.
[41] S. Markov, "Gate leakage variability in nano-CMOS transistors," Ph.D. dissertation, Dept. Electron. Elect. Eng., Univ. Glasgow, Glasgow, U.K., 2009. [Online]. Available: http://theses.gla.ac.uk/771/1/2009markovphd.pdf
[42] F. Giustino, A. Bongiorno, and A. Pasquarello, "Equivalent oxide thickness of a thin oxide interlayer in gate insulator stacks on silicon," *Appl. Phys. Lett.*, vol. 86, no. 19, p. 192901, 2005.
[43] D. A. Muller, T. Sorch, S. Moccio, F. H. Baumann, K. Evans-Lutterodt, and G. Timp, "The electronic structure at the atomic scale of ultrathin gate oxides," *Nature*, vol. 399, pp. 758–761, Jun. 1999.
[44] J. B. Neaton, D. A. Muller, and N. W. Ashcroft, "Electronic properties of the $Si/SiO_2$ interface from first principles," *Phys. Rev. Lett.*, vol. 85, no. 6, pp. 1298–1301, 2000.
[45] F.-A. Fortin, F.-M. De Rainville, M.-A. Gardner, M. Parizeau, and C. Gagné, "DEAP: Evolutionary algorithms made easy," *J. Mach. Learn. Res.*, vol. 13, pp. 2171–2175, Jul. 2012.
[46] O. Madelung, Ed., *Semiconductors: Group IV Elements and III–V Compounds*. New York, NY, USA: Springer-Verlag, 1991.
[47] J. Oh *et al.*, "Chemical structure of the ultrathin $SiO_2$/Si(100) interface: An angle resolved Si $2p$ photoemission study," *Phys. Rev. B*, vol. 63, no. 20, p. 205310, 2001.
[48] R. Buczko, S. J. Pennycook, and S. T. Pantelides, "Bonding arrangements at the $Si\text{-}SiO_2$ and $SiC\text{-}SiO_2$ interfaces and a possible origin of their contrasting properties," *Phys. Rev. Lett.*, vol. 84, no. 5, pp. 943–946, 2000.
[49] R. L. Mozzi and B. E. Warren, "The structure of vitreous silica," *J. Appl. Crystallogr.*, vol. 2, pp. 164–172, Oct. 1969.
[50] F. Giustino, A. Bongiorno, and A. Pasquarello, "Atomistic models of the Si(100)–$SiO_2$ interface: Structural, electronic and dielectric properties," *J. Phys., Condensed Matter*, vol. 17, no. 21, pp. S2065–S2074, 2005.

**Stanislav Markov** (M'09) received the Ph.D. degree in electrical and electronics engineering from the University of Glasgow, U.K., in 2009.

He was with the Device Modeling Group, University of Glasgow, where he studied CMOS device variability until 2012. He has been with the Department of Chemistry, The University of Hong Kong, since 2012, where he has focused on atomic level modeling of nanoscale devices.

**Balint Aradi,** photograph and biography not available at the time of publication.

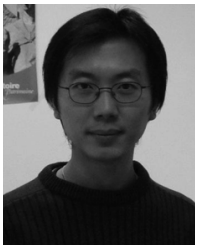

**Chi-Yung Yam** received the Ph.D. degree in chemistry from the University of Hong Kong, Hong Kong, in 2004.

He joined the Beijing Computational Science Research Center, Beijing, China, in 2013, as an Assistant Professor. His current research interests include the development of linear-scaling quantum mechanical methods, quantum transport, and electronic device simulations.

**Hang Xie** received the B.S. and M.S. degrees from Fudan University, Shanghai, China, in 2001 and 2004, respectively, and the Ph.D. degree in physics from the Hong Kong University of Science and Technology, Hong Kong, in 2008.

He completed the post-doctoral training with the Hong Kong University of Science and Technology in 2010. He has been a Post-Doctoral Research Fellow with the Department of Chemistry, University of Hong Kong, Hong Kong, since 2010.

**Thomas Frauenheim,** photograph and biography not available at the time of publication.

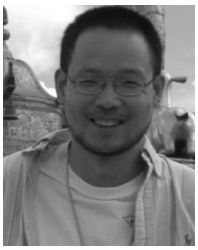

**Guanhua Chen** received the Ph.D. degree in physics from the California Institute of Technology, Pasadena, CA, USA, in 1992.

He joined the University of Hong Kong, Hong Kong, in 1996, where he is currently a Professor and the Head of the Department of Chemistry.

Prof. Chen has been a fellow of American Physical Society since 2014.